



## Research Article

# Air Quality Assessment for Kunooz Gabbro Quarry in Oman: Assessment of PM<sub>10</sub>

Sabah Abdul-Wahab<sup>a\*</sup>, Isra Osman<sup>a</sup>, and Nasser Al-Shukailli<sup>a</sup>

<sup>a</sup> Department of Mechanical and Industrial Engineering, Sultan Qaboos University, Sultanate of Oman

## Article Info

### Article history

**Received:** 31.07.2022

**Revised:** 19.10.2022

**Accepted:** 02.11.2022

### Keywords:

CALPUFF,  
Simulation,  
Modelling,  
Environment,  
Emissions

## ABSTRACT

This study provided an air quality assessment for Kunooz Gabbro Quarry in Al Jaffnain, Al-Seeb, Oman and focused mainly on emitted particulate matter 10 micrometers or less in diameter (PM<sub>10</sub>) from different sources inside the plant. Dispersion of PM<sub>10</sub> was modeled using CALPUFF software. PM<sub>10</sub> particle emissions were modeled for the winter and the summer season. The results of the simulation showed that during the winter season, the maximum one-hour average PM<sub>10</sub> concentration occurred at the center of the quarry and was about 4,957 µg/m<sup>3</sup>. During the summer season, the maximum one-hour average PM<sub>10</sub> concentration occurred at the center of the quarry and was about 4,970 µg/m<sup>3</sup>. All the observed PM<sub>10</sub> concentrations during the summer and winter seasons exceeded the allowable one-hour average concentration of the Environmental Protection Agency (EPA) which is 365.21 µg/m<sup>3</sup>.

## 1. Introduction

Quarrying involves drilling, blasting, loading, unloading, crushing, and screening useful materials to extract them from the Earth. Quarrying products include marble, limestone, gabbro, granite, gypsum, clay, coal, and many others and are used for agricultural, industrial, and domestic purposes. [1]

Unfortunately, quarrying activities can greatly affect the environment because extracting stone depends enormously on explosives and heavy machines, both of which are associated with noise, air, and water pollution, as well as habitat destruction and damage to biodiversity. [2] The most notable form of pollution resulting from stone cutting and quarrying activities is air pollution. Quarrying activities can emit particulate matter (PM) with a diameter 1–75 µm. The degree of pollution from the quarrying activities depends on the composition and the dust particles' size and concentration in the surrounding air, and the local microclimatic conditions. Stone cutting and quarrying industries can lead to many environmental effects, including destruction of natural flora, landscape degradation, ecological disturbance, instability of soil and rock masses, and pollution of air, land and water. [3]

Coarse particles with an aerodynamic diameter equal to or less than 10 micrometers are known as PM<sub>10</sub>. PM is particle pollution and consists of both liquid and solid particles in the air. These particles have a lifespan which is inversely proportional to the particle's diameter. Particles with large diameters can travel up to 30 km while smaller particles may

travel to more than a thousand kilometers. [4] PM is considered toxic and harmful to humans due to its effects on the human body. It can cause irregular heartbeat, heart attacks and lung diseases and is one of the main causes of lung cancer and adverse pregnancy outcomes. Research has shown that PM<sub>10</sub> causes respiratory syncytial virus [5] and might lead to mental and neurological issues. [6].

PM contains hundreds of chemicals that may differ from one industrial application to another. Copper (Cu), iron (Fe) and zinc (Zn) commonly exist in non-tailpipe emission in vehicles, while nickel (Ni) and vanadium (V) are emitted in mixed oil burning industries. Sulfur (S) indicating long-range transport, silicon (Si) is associated with crustal material industries, and potassium (K) is emitted during biomass burning. [7] Some of these chemicals could damage the central nervous system and, with the small size of these particles, they may penetrate the lungs and reach the bloodstream in humans.

Society's rising concerns about industrial areas meeting air quality standards designed to protect human health has resulted in methodologies and tools which perform reliable calculations that can provide transparent decision making. [8] Atmospheric dispersion models are a useful way to estimate pollutant concentrations in the air over a specified period of time. These models can integrate the latest knowledge about atmospheric dynamics and predict dispersal patterns as well as pollutant deposition and chemical transformation. [8]

CALPUFF modelling software has been approved by the U.S. Environmental Protection Agency (EPA) to simulate air pollutant dispersion. The system analyses air quality by

\*Corresponding author: Sabah Abdul-Wahab

\*E-mail address: sabah1@squ.edu.om

<https://doi.org/10.56158/jpte.2022.29.1.02>



simulating the dispersion of pollutants which are generated from sources such as traffic, landfills, and industrial plants. The software depends on meteorological data and the geography of the location under study in simulating the dispersion of pollutants. [9] Previous research has employed CALPUFF software to study the dispersion of pollutants from different sources. For instance, Abdul-Wahab et al. [10] used CALPUFF modelling software to investigate PM<sub>10</sub> along with carbon monoxide (CO), nitrogen oxides (NO<sub>x</sub>) and sulfur dioxide (SO<sub>2</sub>) released from a steel melting plant in Muscat, Oman. Pollutant emissions were modelled on two days, with one representing the summer period and the other representing winter. The results of the simulation showed that all emitted pollutants other than NO<sub>x</sub> were within the U. S. EPA standards.

Joneidi et al. [11] used HOMER software to investigate the dispersion of SO<sub>2</sub> (sulfur dioxide) and CO (carbon monoxide) emitted from District 7 of Tehran Municipality. Using September 30, 2012, as the modelling day, the simulation showed that SO<sub>2</sub> and CO emissions were lower than the EPA's National Ambient Air Quality Standards (NAAQS) and Iranian Ambient Air Standards for CO and SO<sub>2</sub>.

Rojano et al. [12] used CALPUFF software to study the impact of different coal storage areas on nearby communities in terms of PM<sub>10</sub> emissions. In this study, researchers considered the PM<sub>10</sub> emitted during loading, unloading, and hauling of coal, wind disturbances to the surface of the coal, and tractor operations. The results of the study showed that the highest concentrations of PM<sub>10</sub> were reached near emission sources. However, these concentrations did not exceed national standards.

Abdul-Wahab et al. [9] conducted a study using CALPUFF software to analyze the PM<sub>10</sub> emitted from two different processes in a hot-dip galvanizing plant in Oman. PM<sub>10</sub> emissions were modeled on two days to simulate summer and winter periods. The results of the simulation showed that the concentration of the emitted PM<sub>10</sub> was higher during the winter. However, the PM<sub>10</sub> emitted during the modelled summer and winter days did not exceed United States Environmental Protection Agency (U.S. EPA) standards.

In addition, several studies adopted the topic of the simulation of air pollutants using CALPUFF model in different seasons similar to what is achieved in this study for example Pratama [13] conducted a study to investigate air pollution dispersion from kiln stack during the dry and wet seasons using CALPUFF. The study focused on SO<sub>2</sub> emitted by kiln stacks in PT Semen Padang, Tbk. It was observed that the direction of dispersion was influenced by the effect of the land breeze and sea breeze. During the dry season, the pollutants dispersed more toward the urban area compared to the wet season and the pollutant concentration was higher during the dry season. In addition, the recorded concentration levels were below the national quality standard in Indonesia which is 365 µg/m<sup>3</sup>.

Xie et al. [14] used CALPUFF model to predict the concentrations of SO<sub>2</sub>, NO<sub>x</sub>, and PM<sub>2.5</sub> emitted by 31 brick and tile enterprises based on established emission. The hourly average concentrations of NO<sub>x</sub>, SO<sub>2</sub>, and PM<sub>2.5</sub> were simulated during spring, summer, autumn, and winter seasons. The results of the simulation showed that in the summer season there was a large range of pollutant dispersion. However, the range of pollutant dispersion in the winter was smaller.

Abdul-Wahab et al. [15] carried out a study using

CALPUFF to investigate the emission of NO<sub>2</sub>, CO, PM<sub>10</sub> from a Liquefied Natural Gas (LNG) plant located in Oman during the summer and winter seasons. The results of the study showed that the recorded one-hour average concentration of NO<sub>2</sub> during the summer and winter seasons exceeded the U.S. EPA concentration limits. However, the one-hour average concentrations of PM<sub>10</sub> and CO were within the U.S. EPA's permissible standards.

Also, Otero-Pregigueiro et al. [16] conducted a study to estimate the concentration of the emitted PM<sub>10</sub>-bound manganese from industrial sources in the Santander Bay area, Northern Spain by using CALPUFF. The model was supported by a dataset observation with 101 daily samples from four sites suited in the area of the manganese alloy plant. The results of the simulation showed that the concentration of PM<sub>10</sub>-bound manganese within the area of the study was higher than the standards set by the World Health Organization (WHO) and the U.S. EPA which suggested that the Mn concentrations in the area needed to be reduced. For more studies, refer to [17, 18, 19]

The objective of the current study was to investigate the impact of PM<sub>10</sub> on the environment surrounding the Gabbro Quarry. This environmental impact results from drilling and blasting operations, stone loading and unloading, the three stage of crushing and the two stages of screening and piling in the quarry. For the current study, PM<sub>10</sub> dispersion modeling was accomplished using CALPUFF software for the winter season using data from February 2, 2018, and the summer was represented by data from July 2, 2018. The results of the simulation were compared with PM<sub>10</sub> emission limits set by the U.S. EPA.

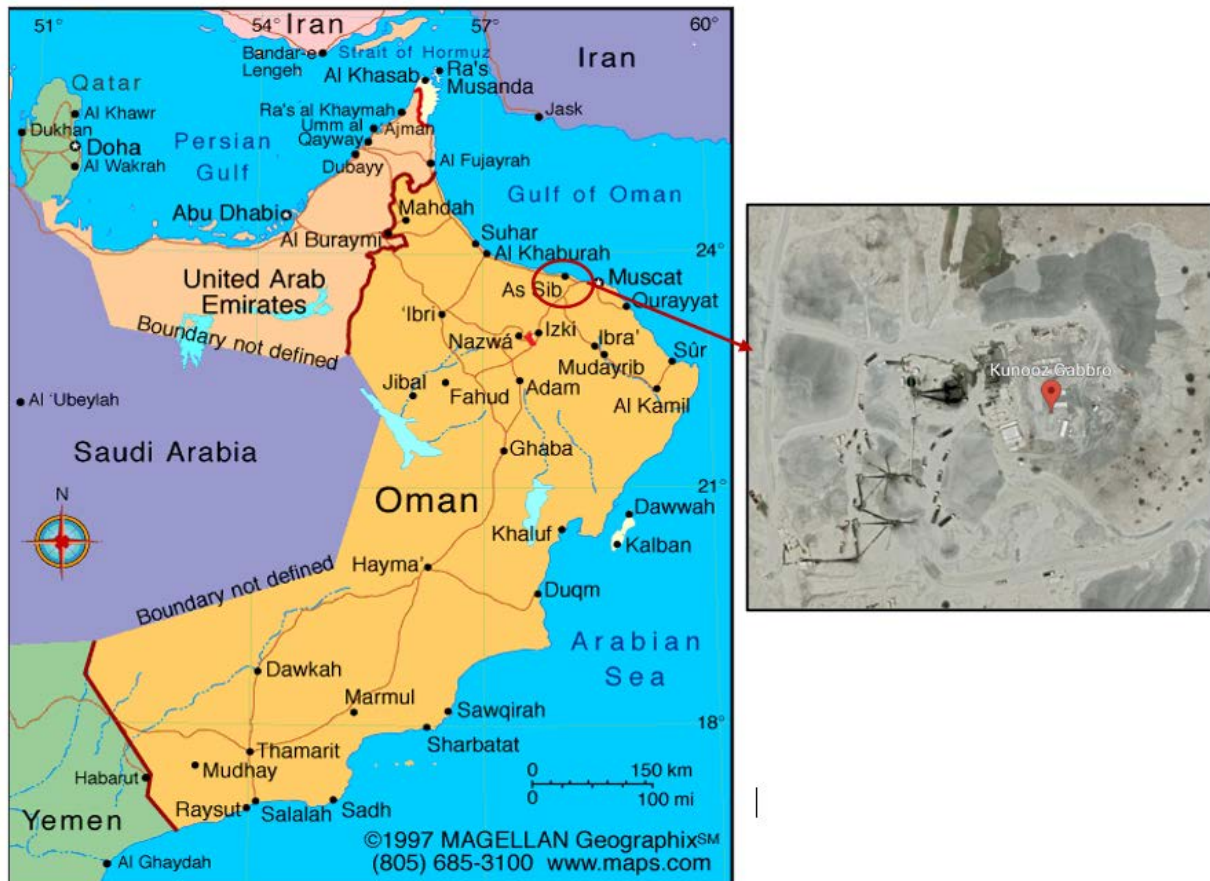
## 2. Materials and Method

### 2.1. Description of the quarry under study

This study was conducted for Kunooz Gabbro Quarry, which is owned by Kunooz Oman Holdings and produces crushed gabbro stones. Figure 1 shows the geographical location of Kunooz Gabbro plant. The plant is located in Al Jaffnain, Al Seeb, Oman, which is about 40 km southwest of Muscat and about five km south-southwest of Al Jiffnain Village. Based on the National Center for Statistics and Information in the Sultanate of Oman, the total population in Al Seeb was 465,607 in 2018. Figure 2 shows a flowchart of the processes carried out inside the plant. The processes inside the quarry involve different stages of crushing and screening which eventually will result in a stone size ranging from 0-40 mm. Table 1 shows a description of the quarrying processes carried out inside the plant. The plant's working hours are from 6:30 AM to 6:00 PM. Overall plant resources are estimated to be 130 million tons with a concession that covers 2.17 km<sup>2</sup>. [20] The company was assigned a gabbro mining lease; in 2010, the first mining report was prepared; and actual mining activities commenced in 2012. The development of the whole site, including access roads and electrical lines and transformers, was completed within a 12-month period. After a couple of experimental runs and product evaluation, the plant's commercial operations started in May 2013. The produced gabbro supplies road and construction companies. [21] The quarry is the leading producer of gabbro stones in Oman, and it is one of the nearest quarries to Muscat city limits. The crusher and quarry are connected to surrounding cities and towns by a well-developed road network. [22]

**Table 1.** Process description

No.	Process	Description
1.	Drilling	More than 100 holes drilled in the mountain in average depth of 10m, a diameter of 76 mm and a spacing of 2.6 m approximately, in order to provide space for the explosives to take place.
2.	Blasting	After placing the explosives in the holes drilled, an explosion was done in the mountain to extract the gabbro rocks. This action is done once a week and the volume of the gabbro rock extracted is around 10000 cubic meters for each blast.
3.	Loading and Unloading (Inside Plant)	Here the gabbro rocks are transported from the quarry to start further processing (Crushing, Screening ...etc.). Around 80 trips with 18 cubic meters tippers are done daily.
4.	Primary Crushing	This is the first step in gabbro stone processing. TRIO JAW Crusher-CT 3254 is used to crush the gabbro rocks that have a diameter up to 700 mm. after this step the crushed stones are transferred to BIN1.
5.	Secondary Crushing	In this step the pre-crushed gabbro stones that were stored in BIN1 are crushed to a maximum of 60 mm diameter with a Cone Crusher TRIO- TC66.
6.	Primary Screening	In this step the 60 mm gabbro stones are divided into 3 categories. The stones between 45 to 60 mm are moved back to BIN1 through a conveyor to be crushed with the cone crusher again. And the ones with diameter less than 5mm (sand) are either stored in the stockpile or transported to the client. The stones from 5-45 mm are transferred to BIN 2. The name of the Screen is TRIO-5143-2-DECK.
7.	Tertiary Crushing	The amount that was stored in BIN2 are then transferred to the VSI TRIO- TV95 for further crushing and then transferred to screen number 2.
8.	Secondary Screening	In this step the gabbro stones are subdivided into five categories depending on the size of the particle. <ul style="list-style-type: none"> <li>✓ 0-5 mm</li> <li>✓ 5-10 mm</li> <li>✓ 10-20 mm</li> <li>✓ 20-40 mm</li> <li>✓ Larger stones</li> </ul> The 0-40 particles are classified as a product for the plant and either transported to client or added to the storage pile. The larger stones are returned to BIN 2 again. The name of the screen is TRIO-6203-3-DECK.
9.	Loading and Unloading (Outside Plant)	This is where the products are transported outside the plant. Around 60 to 70 trips are done daily with 18 cubic meter tippers, 36 cubic meter and 45 cubic meter trailers.
10.	Storage Piles	Where the extra amount of gabbro products stored.

**Figure 1.** Location of Kunooz Gabbro plant

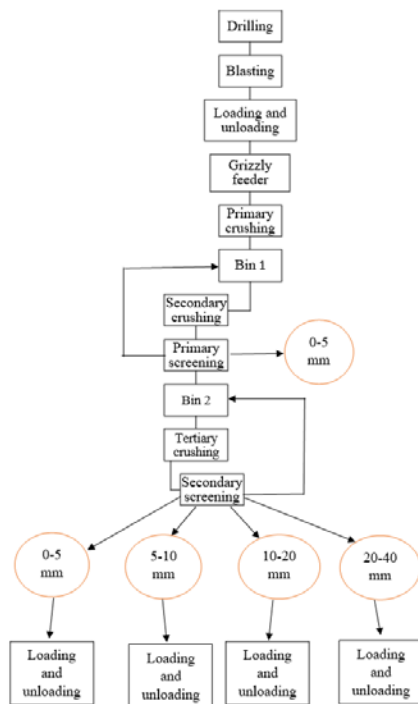


Figure 2. Process flow chart

The nearest healthcare facility is located 5.2 km northeast of the plant, and the nearest school is only 3.9 km south of the plant. Rusayl Industrial Estate (RIE), which is the leading industrial estate in Oman, is located 9.2 km northeast of the plant. The industrial estate occupies 7.9 million m<sup>2</sup> with approximately 211 industrial factories. [10] These factories produce a wide range of products including stationery, chemicals, garments, building materials and paint. [23]

Over the past seven years, Oman's market for aggregates, gravel, and crushed stone has grown steadily. Demand is expected to continue to increase with the continued government investments in tourism projects, housing, infrastructure, and roads. [21] This study was conducted to investigate the level of PM<sub>10</sub> emitted from Kunooz Gabbro Quarry and to discuss its environmental effect due to its proximity to Muscat city limits.

## 2.2. Description/input data for CALPUFF modeling system

### 2.2.1. Meteorological data Surface data

For this study, hourly data on relative humidity, atmospheric pressure, wind direction and speed, cloud cover and height, temperature and precipitation were collected from the Directorate General of Meteorology and Air Navigation's Public in the Authority of -Civil Aviation (PACA). Table 2 shows information about the surface station from which the data was collected. Based on the data available, two days in 2018 were selected to represent the summer and winter seasons: July 2, 2018, was selected to represent summer, and February 2, 2018, was selected to represent winter. The collected data were arranged in a format suitable for CALPUFF's SMERGE program to help convert the raw data into a SURFACE.DAT data file to be further processed in CALMET.

### 2.2.2. Upper air data

The next step was to collect upper air meteorological data from the National Oceanic and Atmospheric Administration/Earth System Research Laboratory (NOAA/ESRL) Radiosonde Database website. [24] Table 2 shows information about the upper air station. The collected

data were for the days selected to represent the winter and summer seasons. The twelve-hour interval upper air data was then prepared to be processed in CALMET by converting the collected data into an UP.DAT data file through CALPUFF's READ62 program.

Table 2. Information of the surface and upper air stations

Parameter	Surface station	Upper Air Station
Station name	Muscat Meteorological station	ABU DHABI INTL 99 AE
Station initials (INIT)	OOMS	OMAA
UTM latitude	23.58°N	24.43 N
UTM longitude	58.28°E	54.65 E
Location X on grid	5 km	-2000 km
Location Y on grid	5 km	200 km
Station elevation	17 m	27 m
Weather Bureau Army Navy (WBAN) station number	99999	99999
World Meteorological Organization (WMO) identifier	41256	41217

### 2.2.3. Emission data

The current study focused on analyzing PM<sub>10</sub> emissions from Kunooz Gabbro Quarry. Each step in the quarrying process can contribute to PM<sub>10</sub> emissions, including line and area sources.

In the current study, drilling, blasting; the primary, secondary, and tertiary crushers; the primary and secondary screens, and stockpiles were considered area sources. Unpaved road #1 and unpaved road #2 were modeled as line sources. Table 3 shows the data used for calculating emission rates, and Table 4 shows the equations used for calculating PM<sub>10</sub> emission rates from each source. Tables 5 and 6 provide a summary of all PM<sub>10</sub> emission data on the plant site and the input data considered in this study. These emission data were used in CALPUFF to model winter and summer PM<sub>10</sub> dispersion.


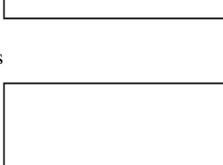
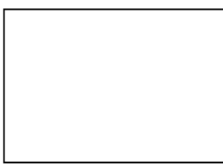
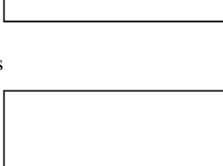

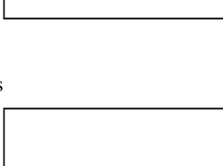
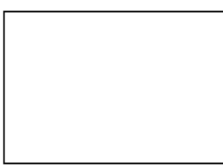
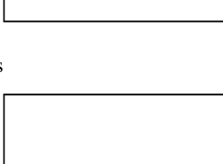
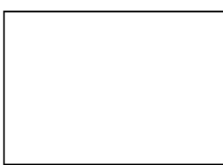


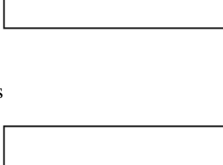
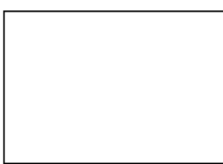


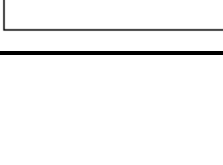
Table 3. Dust sources and required information for calculating emission rates of PM<sub>10</sub>

No.	Unit	Information about each unit
1.	Drilling	Drill diameter = 76 mm Drill depth = 10 m Number of drills per blast = around 150 drill/blast Drilling take about 5 days with 8 working hours/day
2.	Blasting	Volume of Blasting = 10000 m <sup>3</sup> Density of the rocks = 2.5 ton/m <sup>3</sup> Blasting is done once a week
3.	Unpaved Road #1	80 trips done each day Weight of tippers is around 16 ton The Emission is controlled The distance is 900 m The width of the road is 5 m
4.	Primary Crushing	Primary crusher capacity = 350 ton/hour
5.	Secondary Crushing	Secondary crusher capacity = 250 ton/hour
6.	Tertiary Crushing	Tertiary crusher capacity = 200 ton/hour
7.	Primary Screening	Primary screen capacity = 250 ton/hour
8.	Secondary Screening	Secondary screen capacity = 275 ton/hour
9.	Unpaved Road #2	60-70 trips done each day Average weight of tippers and trailers is around 18 ton The Emission is controlled The distance is 3000 m The width of the road is 8 m
10.	Stockpiles	Material transferred = 300 ton/hour

**Table 4.** Equation used for calculating the emission rates of PM<sub>10</sub> from different dust sources.

N O.	Dust Source	Equation for PM <sub>10</sub> Emission Rate
1.	Drilling	$E = EF \left( \frac{lb}{ton} \right) * Capacity\ of\ Drilling \left( \frac{ton}{h} \right) * 454 \left( \frac{g}{lb} \right) * 1 / 3600 \left( \frac{h}{s} \right)$ <p>Where: EF is the emission factor for drilling = 0.00008 Capacity of drilling = 625</p>
2.	Blasting	$E = EF \left( \frac{lb}{ton} \right) * Capacity\ of\ Blasting \left( \frac{ton}{hour} \right) * 454 \left( \frac{g}{lb} \right) * 1 / 3600 \left( \frac{hour}{second} \right)$ <p>Where: EF is the emission factor for blasting = 0.076 Capacity of blasting = 625</p>
3.	Primary Crushing	$E = EF \left( \frac{lb}{ton} \right) * Capacity\ of\ Primary\ Crushing \left( \frac{ton}{hour} \right) * 454 \left( \frac{g}{lb} \right) * 1 / 3600 \left( \frac{hour}{second} \right)$ <p>Where: EF is the emission factor for primary crushing = 0.012 Capacity of primary crushing = 350</p>
4.	Secondary Crushing	$E = EF \left( \frac{lb}{ton} \right) * Capacity\ of\ Secondary\ Crushing \left( \frac{ton}{hour} \right) * 454 \left( \frac{g}{lb} \right) * 1 / 3600 \left( \frac{hour}{second} \right)$ <p>Where EF is the emission factor for secondary crushing = 0.012 Capacity of secondary crushing = 250</p>
5.	Tertiary Crushing	$E = EF \left( \frac{lb}{ton} \right) * Capacity\ of\ Tertiary\ Crushing \left( \frac{ton}{hour} \right) * 454 \left( \frac{g}{lb} \right) * 1 / 3600 \left( \frac{hour}{second} \right)$ <p>Where EF is the emission factor for tertiary crushing = 0.00243 Capacity of tertiary crushing = 200</p>
6.	Primary Screening	$E = EF \left( \frac{lb}{ton} \right) * Capacity\ of\ Primary\ Screening \left( \frac{ton}{hour} \right) * 454 \left( \frac{g}{lb} \right) * 1 / 3600 \left( \frac{hour}{second} \right)$ <p>Where EF is the emission factor for primary screening = 0.0022 Capacity of primary screening = 250 <math>\frac{ton}{hour}</math></p>
7.	Secondary Screening	$E = EF \left( \frac{lb}{ton} \right) * Capacity\ of\ Secondary\ Screening \left( \frac{ton}{hour} \right) * 454 \left( \frac{g}{lb} \right) * 1 / 3600 \left( \frac{hour}{second} \right)$ <p>Where EF is the emission factor for secondary screening = 0.0022 Capacity of secondary screening = 275</p>
8.	Crushing Storage Piles	$E = EF \left( \frac{lb}{ton} \right) * Material\ Transferred \left( \frac{ton}{hour} \right) * 454 \left( \frac{g}{lb} \right) * 1 / 3600 \left( \frac{hour}{second} \right)$ <p>Where EF is the emission factor for crushing storage piles = 0.12 Material transferred = 258 <math>\frac{ton}{hour}</math></p>
9.	Unpaved Road #1	$E = K * \left( \frac{S}{12} \right)^a * \left( \frac{W}{3} \right)^b \left( \frac{lb}{VMT} \right) * 454 \left( \frac{g}{lb} \right) * 0.621 \left( \frac{mile}{KM} \right) * number\ of\ trips * Distance\ Travelled\ per\ trip(km) * (1 - \% \text{ Control of dust emissions}) * \frac{1}{3600} \left( \frac{hour}{sec} \right)$ <p>Where: K (particle size multiplier) = 4.9 S (silt content) = 8.3 W (weight of empty truck) = 15.37 a = 0.7 b = 0.45 Number of trips = 80 Distance travelled per trip = 0.9 % control of dust emissions = 80</p>
10.	Unpaved Road #2	$E = K * \left( \frac{S}{12} \right)^a * \left( \frac{W}{3} \right)^b \left( \frac{lb}{VMT} \right) * 454 \left( \frac{g}{lb} \right) * 0.621 \left( \frac{mile}{KM} \right) * number\ of\ trips * Distance\ Travelled\ per\ trip(km) * (1 - \% \text{ Control of dust emissions}) * \frac{1}{3600} \left( \frac{hour}{sec} \right)$ <p>Where K (particle size multiplier) = 4.9 S (silt content) = 8.3 W (weight of empty truck) = 18.2 a = 0.7 b = 0.45 Number of trips = 65 Distance travelled per trip = 3 % control of dust emissions = 80</p>

**Table 5.** Area source input parameters

Area points	Parameter	Drilling
Point B  Point A	Point A (upper right)	-70.51 m, 249 m
	Point B (upper left)	-89.31 m, 294.16 m
	Point C (lower left)	-88.99 m, 256.95 m
	Point D (lower right)	-70.82 m, 257.28 m
	Emission rate	0.006305 g/s
	Effective height	10 m
Point C  Point D	Base elevation	145 m
	Initial sigma Z	4.7
Area points	Parameter	Blasting
Point B  Point A	Point A (upper right)	-70.51 m, 249 m
	Point B (upper left)	-89.31 m, 294.16 m
	Point C (lower left)	-88.99 m, 256.95 m
	Point D (lower right)	-70.82 m, 257.28 m
	Emission rate	5.99 g/s
	Effective height	10 m
Point C  Point D	Base elevation	145 m
	Initial sigma Z	4.7
Area points	Parameter	Primary Crusher
Point B  Point A	Point A (upper right)	-80 m, -34 m
	Point B (upper left)	-95 m, -34 m
	Point C (lower left)	-95 m, -40 m
	Point D (lower right)	-80 m, -40 m
	Emission rate	0.0529 g/s
	Effective height	4 m
Point C  Point D	Base elevation	145 m
	Initial sigma Z	1.9
Area points	Parameter	Primary Screen
Point B  Point A	Point A (upper right)	-23.265 m, -7.875 m
	Point B (upper left)	-32.265 m, -7.875 m
	Point C (lower left)	-32.265 m, -11.383 m
	Point D (lower right)	-23.265 m, -11.383 m
	Emission rate	0.0694 g/s
	Effective height	4 m
Point C  Point D	Base elevation	145 m
	Initial sigma Z	1.9
Area points	Parameter	Secondary Crusher
Point B  Point A	Point A (upper right)	-49.065 m, -5.265 m
	Point B (upper left)	-55.065 m, -5.265 m
	Point C (lower left)	-55.065 m, -13.465 m
	Point D (lower right)	-49.065 m, -13.465 m
	Emission rate	0.0378 g/s
	Effective height	4 m
Point C  Point D	Base elevation	145 m
	Initial sigma Z	1.9
Area points	Parameter	Secondary Screen
Point B  Point A	Point A (upper right)	-15.454 m, 28.185 m
	Point B (upper left)	-26.454 m, 28.185 m
	Point C (lower left)	-26.454 m, 13.465 m
	Point D (lower right)	-15.454 m, 13.465 m
	Emission rate	0.0763 g/s
	Effective height	4 m
Point C  Point D	Base elevation	145 m
	Initial sigma Z	1.9
Area points	Parameter	Tertiary Crusher
Point B  Point A	Point A (upper right)	-43.934 m, 29.185 m
	Point B (upper left)	-40.434 m, 29.185 m
	Point C (lower left)	-40.434 m, 22.685 m
	Point D (lower right)	-43.934 m, 22.685 m
	Emission rate	0.0613 g/s
	Effective height	4 m
Point C  Point D	Base elevation	145 m
	Initial sigma Z	1.9
Area points	Parameter	Stockpiles
Point B  Point A	Point A (upper right)	-36.39 m, 59.73 m
	Point B (upper left)	-67.55 m, 60.19 m
	Point C (lower left)	-66.92 m, 27.9 m
	Point D (lower right)	-34.81 m, 28.93 m
	Emission rate	3.91 g/s
	Effective height	3 m
Point C  Point D	Base elevation	145 m
	Initial sigma Z	1.4 m



**Table 6.** Input data for emission sources for CALPUFF

Line Sources								
Source Description	Length of side (m)	Release HAG (m)	x Coord starting (m)	y Coord starting (m)	x Coord ending (m)	y Coord ending (m)	PM <sub>10</sub> Emission Rate (g/s)	
Unpaved Road #1	5	3.5	0	0	-20	490	8.9049	
Unpaved Road #2	8	3.5	0	0	1165	2030	26.0232	
Area Sources								
Source Description	Corner A	Corner B	Corner C x (m) y (m)	Corner D x (m) y (m)	HAG (m)	Area (m <sup>2</sup> )	PM <sub>10</sub> Emission Rate (g/s)	PM <sub>10</sub> Emission Rate g/s m <sup>2</sup>
Drilling	(-70.51, 294.5)	(-89.31, 294.16)	(-88.99, 256.94)	(-70.82, 257.28)	10	660.6	0.006305	0.0000954
Blasting	(-70.51, 294.5)	(-89.31, 294.16)	(-88.99, 256.94)	(-70.82, 257.28)	10	660.6	5.99	0.00907
Primary Crusher	(-80, -34)	(-95, -34)	(-95, -40)	(-80, -40)	4	90	0.0529	0.000588
Primary Screen	(-23.265, -7.875)	(-32.265, -7.875)	(-32.265, -11.383)	(-23.265, -11.383)	4	36	0.0694	0.00193
Secondary Crusher	(-49.065, -5.265)	(-55.065, -5.265)	(-55.065, -13.465)	(-49.065, -13.465)	4	49.2	0.0378	0.000768
Secondary Screen	(-15.454, 28.185)	(-26.454, 28.185)	(-26.454, 23.685)	(-15.454, 23.685)	4	49.5	0.0763	0.00154
Tertiary Crusher	(-43.934, 29.185)	(-40.434, 29.185)	(-40.434, 22.685)	(-43.934, 22.685)	4	29.25	0.0613	0.0021
Stockpiles	(-36.39, 59.73)	(-67.55, 60.19)	(-66.92, 27.9)	(-34.81, 28.93)	3	923	3.91	0.00423

### 2.3.Operation of CALPUFF modeling system

CALPUFF modeling software is a non-steady multilayer dispersion model advised by the U.S. EPA to model air quality. The software is used globally as a predictive air quality model for different gaseous emissions and provides a clear image of pollutant concentrations in the atmosphere during selected time periods. The software comprises three primary components: CALMET, CALPUFF and CALPOST. CALMET is basically a diagnostic three-dimensional (3D) meteorological model which provides, hourly readings of wind and temperature fields. Location-dependent observational data are required to be inputted in CALMET, and these data include both upper air and surface meteorological data. Other than meteorological data, CALMET needs geophysical data from the terrain and land use of the study area. CALPUFF is used to generate temporal and spatial effects of meteorological conditions on the removal and transportation of gaseous emissions from various sources to the surroundings. CALPOST provides the simulation results of the specified pollutants by processing CALPUFF's output files. [10, 25, 26]

For the current study, the meteorological grid's shared information (Table 7) was input into a common file through the identified shared information module. This data is shared by all CALPUFF processors. For this simulation, a 16-bit Windows XP computer with 1 GB RAM and an Intel Pentium 4 3.4 GHz processor was used. The fractional convergence criteria for numerical area source and numerical slug sampling integration were set at 1.0E-6 and 1.0E-04, respectively.

**Table 7.** CALPUFF input information for the study area

Parameter	Kunooz Gabbro
Projection	LCC
LCC latitude of origin	23.5019 N
LCC longitude of origin	58.1687 E
Latitude 1	7 N
Longitude 2	36 N
False easting	0

False northing	0
Continent/ocean	Global
Geoid-ellipsoid	WGS-84: WGS 84
Region	Global coverage [WGS-84 reference ellipsoid and geoid
Datum code	WGS-84
X (easting) (km)	-60
Y (northing) (km)	-60
Number of X grid cells	100
Number of Y grid cells	100
Grid spacing (km)	1
Number of vertical layers	10
Cell face heights (m)	0, 20, 40, 60, 80, 160, 320, 640, 1000, 2200, 3000
Base time zone	UTC +04:00
Hemisphere	Northern

## 3. Results and Discussion

### 3.1.Analysis of the wind roses

Figures 3 and 4 demonstrate the wind roses for the winter and summer modeling days. The wind rose shows the wind speed and direction in the location under study. The length of the spoke shows the frequency of the wind. The different colors appearing on the spoke indicate the ranges of wind speed during the day. For example, the longest spoke shows the wind direction with the highest frequency, and the longest color appearing on the stroke indicates the predominant wind speed [27].

SURF.DAT: (Station ID = 99999), Height = 10.0 m, [2018 2 2 1 2018 2 2 23]  
Annual(J-D): Total Hours = 23, Valid Hours = 23 [Valid = 100%], Calm Hours = 0

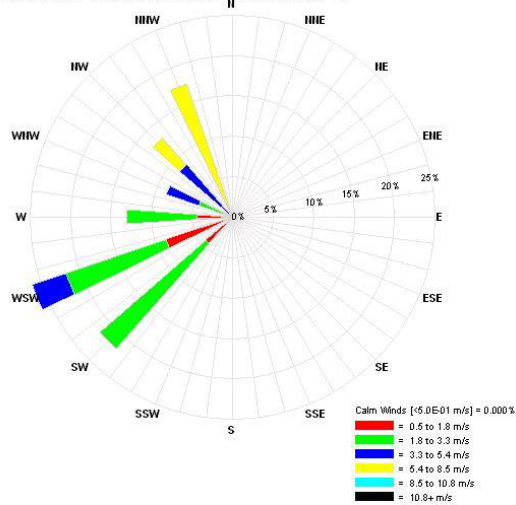


Figure 3. Wind rose for February 2, 2018

On February 2, 2018, the wind blew from southwest to north-northwest and generally it appeared to move at between 0.5 to 8.5 m/s (1800 to 30600 m/hr). The most dominant wind blew from the west-southwest (WSW) at a speed ranging between 0.5–5.4 m/s (1800 to 19440 m/hr). The second most dominant wind below from southwest (SW) at a speed ranging from 0.5 to 3.3 m/s. The third most dominant wind below from north-northwest (NNW) at a speed ranging from 5.4 to 8.5 m/s (19440 to 30600 m/hr). The least dominant wind below from west-northwest (WNW) at a speed ranging between 1.8 to 5.4 m/s (6480 to 19440 m/hr).

On July 2, 2018, the most dominant wind blew from the northeast (NE) at a speed ranging from 0.5 to 8.5 m/s (1800 to 30600 m/hr), and from east-northeast (ENE) at a speed ranging from 0.5 to 5.4 m/s (1800 to 19440 m/hr) as shown in Figure 4. The winds from the other directions were less frequent and appeared to move with an average speed between 0.5 to 8.5 m/s (1800 to 30600 m/hr) at different distances from the quarry.

SURF.DAT: (Station ID = 99999), Height = 10.0 m, [2018 7 2 1 2018 7 2 23]  
Annual(J-D): Total Hours = 23, Valid Hours = 23 [Valid = 100%], Calm Hours = 2

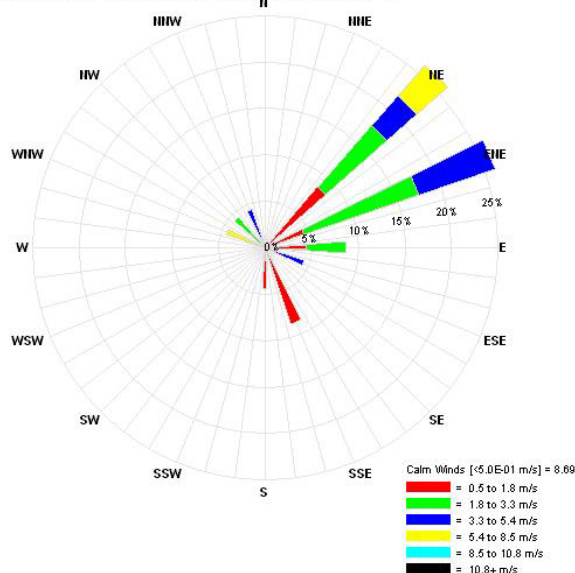


Figure 4. Wind rose for July 2, 2018

### 3.2. Average concentration level

#### Winter average concentrations (February)

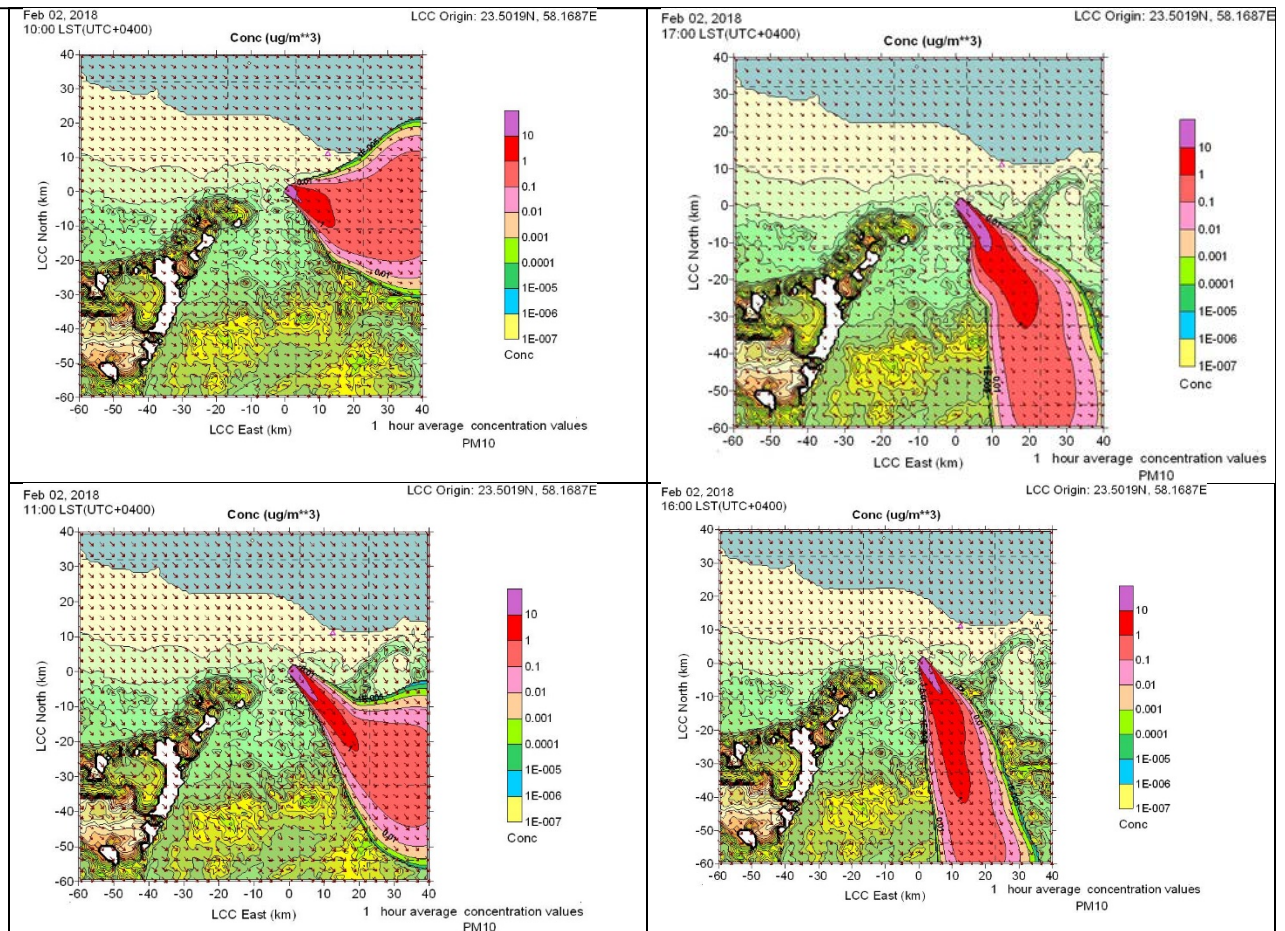
The modelling day February 2, 2018 was selected to represent the winter season. Table 8 shows the top 10 highest one-hour average concentration of PM<sub>10</sub> simulated on February 2, 2018 from 00:00 to 23:00 local standard time (LST). The maximum one-hour average PM<sub>10</sub> concentration of 4,957 µg/m<sup>3</sup> occurred at 17:00 LST at the center of the quarry. The second highest PM<sub>10</sub> concentration was 4,324 µg/m<sup>3</sup> and occurred at 00:00 LST 0.5 km east and 0.5 km north of the center of the plant. The third highest PM<sub>10</sub> concentration was 3,265 µg/m<sup>3</sup> and occurred at 16:00 LST at the center of the plant. The fourth highest PM<sub>10</sub> concentration was 2,764 µg/m<sup>3</sup> which occurred at 11:00 LST at the center of the plant as well. Thus, it can be observed that the highest concentrations of PM<sub>10</sub> were generally found close to the center. Figure 5 shows the contour plots of the plume trajectories of the four highest one-hour average PM<sub>10</sub> concentrations on February 2, 2018. The plumes direction at 10:00, 11:00, 16:00, and 17:00 LST were influenced by the wind coming from southwest to north-northwest directions in the specified day of February 2, 2018, which resulted in the plumes to disperse away from the sea in an eastward direction at 10:00 LST and 11:00 LST and eventually heading far away from the sea toward a southward direction at 16:00 LST and 17:00 LST. In addition, the effect of the sea breeze played a role in directing the pollutants toward the land at 11:00, 16:00, and 17:00 LST which caused the plume trajectories to be directed toward the land and away from the sea.

Table 8. List of top 10 1-h average PM<sub>10</sub> concentrations simulated on February 2, 2018 from 00:00 to 23:00

1-h average PM <sub>10</sub> concentration				Allowed 1-hour average concentration* (µg/m <sup>3</sup> )
No.	Time (HH:MM)	Concentration (µg/m <sup>3</sup> )	Coordinates (km)	
1	17:00	4957	0.0,0.0	365.21 µg/m <sup>3</sup>
2	00:00	4324	0.5,0.5	
3	16:00	3265	0.0,0.0	
4	11:00	2764	0,0	
5	00:00	2461	0,0	
6	10:00	2290	0,0	
7	20:00	2197	0,0.5	
8	02:00	2058	0.5,0.5	
9	22:00	1589	0,0.5	
10	02:00	1471	0,0	

\* U.S. Environmental Protection Agency [28]





**Figure 5.** Contour plots showing the plume trajectory of the first (top left), second (top right), third (bottom left), and fourth (bottom right) highest 1-h average PM<sub>10</sub> concentrations on February 2, 2018

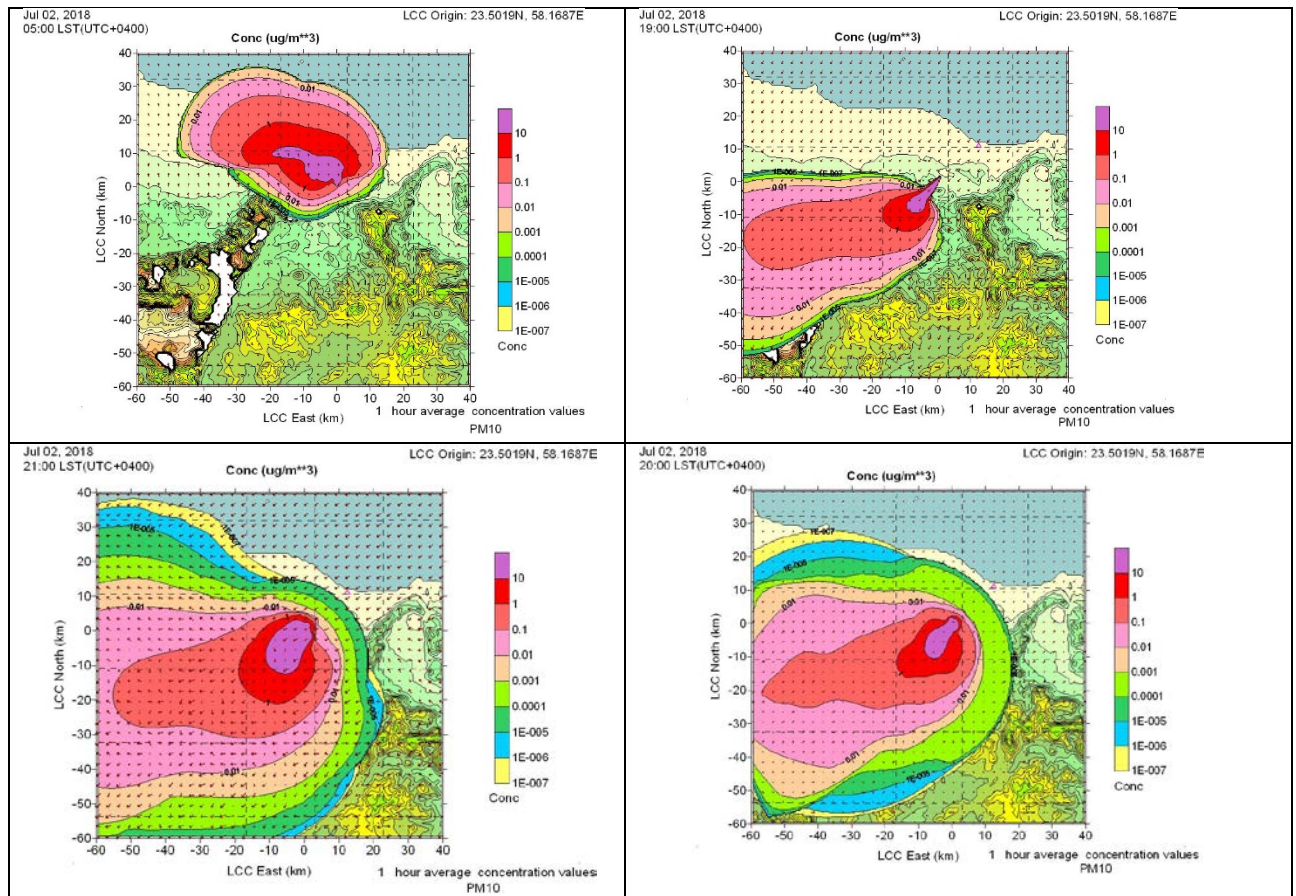
#### Summer average concentrations (July)

The modelling day July 2, 2018 was selected to represent the summer season. Table 9 shows the top 10 one-hour average concentrations of PM<sub>10</sub> simulated on July 2, 2018, from 00:00 to 23:00 LST. The maximum one-hour average PM<sub>10</sub> concentration (4,970 µg/m<sup>3</sup>) occurred at 19:00 LST exactly at the center of the quarry. The second highest PM<sub>10</sub> concentration was 4,715 µg/m<sup>3</sup> and occurred at 5:00 LST 0.5 km north of the quarry. The third highest PM<sub>10</sub> concentration was 4,468 µg/m<sup>3</sup> and occurred at 20:00 LST at the center of the quarry. The fourth highest PM<sub>10</sub> concentration was 4337 µg/m<sup>3</sup> and occurred at 20:00 at 0.5 km east and 0.5 north of the center of the quarry. Figure 6 shows the contour plots of the plume trajectories of the four highest one-hour average PM<sub>10</sub> concentrations on July 2, 2018 at 05:00, 19:00, 20:00, and 21:00 LST. It can be observed that the plume trajectory recorded at 5:00 close to the plant started to move toward a westward direction. The rest of the plume trajectories were very much influenced by the sea breeze as the recorded plume trajectories at 19:00, 20:00, and 21:00 LST dispersed toward the land completely in a westward direction and concentrated in the surrounding domain as the most dominant wind were coming from the NE and ENE directions in this day. As can be seen, the effect of the land breeze was very minimal during this day.

**Table 9.** List of top 10 1-h average PM<sub>10</sub> concentrations simulated on July 2, 2018 from 00:00 to 23:00.

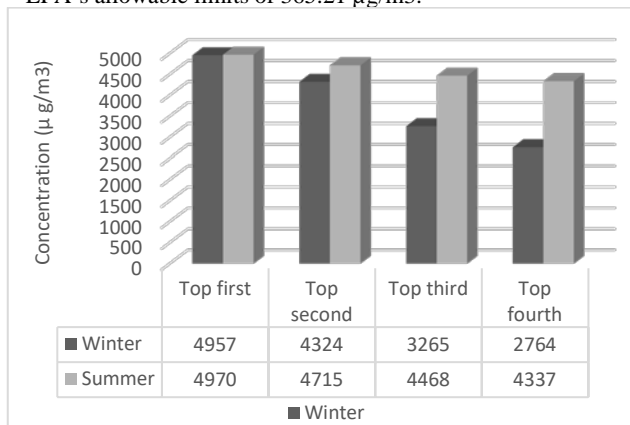
1-h average PM <sub>10</sub> concentration				
No	Time (HH:MM)	Concentration (µg/m <sup>3</sup> )	Coordinates (km)	Allowed 1-hour average concentration *
				(µg/m <sup>3</sup> )
1	19:00	4970	0,0	365.21 µg/m <sup>3</sup>
2	05:00	4715	0,0.5	
3	20:00	4468	0,0	
4	20:00	4337	0.5,0.5	
5	20:00	3979	0,0.5	
6	19:00	3261	-0.5,-0.5	
7	08:00	2707	0,0	
8	04:00	2703	-0.5,1.5	
9	02:00	2244	-1.5,0.5	
10	03:00	1956	-1,-0.5	

\* U.S. Environmental Protection Agency [29]



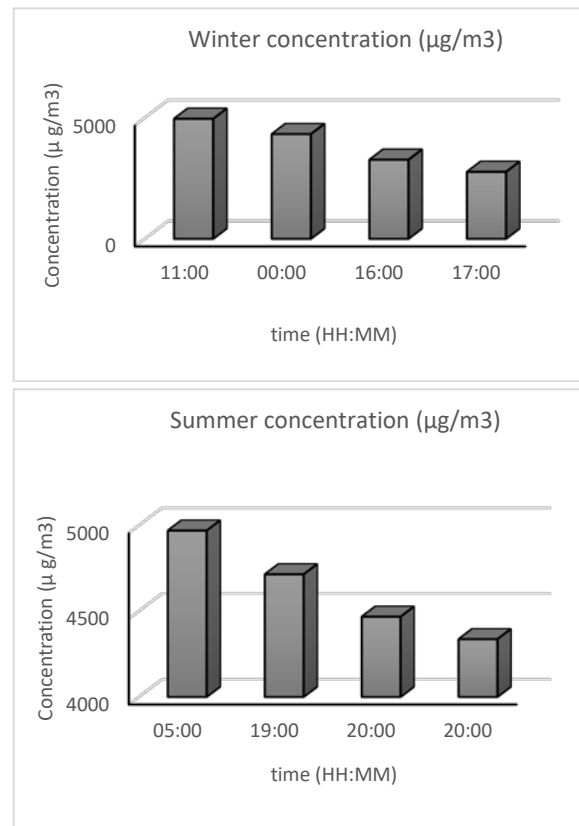
**Figure 6.** Contour plots showing the plume trajectory of the first (top left), second (top right), third (bottom left), and fourth (bottom right) highest 1-h average  $PM_{10}$  concentrations on July 2, 2018

Figure 7 shows a comparison between the  $PM_{10}$  concentration levels emitted during the summer and winter seasons. It can be observed that the concentration of  $PM_{10}$  was higher during the summer season (July 2, 2018) than the winter season (February 2, 2018). However, both the concentration of  $PM_{10}$  in the summer and winter seasons exceeded the U.S. EPA's allowable limits of  $365.21 \mu g/m^3$ .



**Figure 7.** Comparison between  $PM_{10}$  concentration emitted from the quarry in the summer and winter seasons

Figure 8 shows the top four  $PM_{10}$  concentration emitted from the quarry in the summer and winter seasons according to the time. As can be seen, the top four concentration during the summer and winter seasons were recorded at different times in which the highest  $PM_{10}$  concentration during the winter was recorded at 11:00 LST and the highest  $PM_{10}$  concentration during the summer was recorded at 5:00 LST.



**Figure 8.** Top four  $PM_{10}$  concentration emitted from the quarry in the summer and winter seasons according to the time



#### 4. Conclusion

This study was conducted for Kunooz Gabbro Quarry in which CALPUFF simulation model was used to investigate the concentrations of PM<sub>10</sub> emitted from different sources inside the plant which were identified as area and line sources and the meteorological data were entered in the software in order to simulate the dispersion of pollutants from the quarry. The results of the simulation using CALPUFF software showed that the maximum one-hour average PM<sub>10</sub> concentrations during the summer season was higher compared to the concentrations observed in the winter season. The top 3 highest concentrations recorded in the winter season (February 2, 2018) were 4,957 µg/m<sup>3</sup>, 4,324 µg/m<sup>3</sup>, and 3,265 µg/m<sup>3</sup>, respectively. However, the top 3 highest concentrations recorded in the summer season (July 2, 2018) were 4,970 µg/m<sup>3</sup>, 4,715 µg/m<sup>3</sup>, and 4,468 µg/m<sup>3</sup>, respectively. It should be noted that, during both seasons the highest one-hour average PM<sub>10</sub> concentration occurred at the center of the quarry. When comparing the highest one-hour concentrations for both seasons with the U.S. EPA standards, both seasons' levels were significantly higher than the common standards set by the U.S. EPA at 365.21 µg/m<sup>3</sup>. In addition, the strong influence of the sea breeze in the summer and winter resulted in plumes dispersing over the land, causing them to concentrate within the plant's domain, these high PM<sub>10</sub> concentrations, therefore, may cause health issues for the people working in the plant as well as the people who live near the plant. It is recommended that Kunooz Gabbro Quarry control their emissions and improve their dust management plan.

The limitations of this study can be summarized as the study covered two modelling days which represent each of the summer and winter seasons. In addition, the results of the study were not compared with actual measured data from the sites as they were not available. For future work and enhancement of the study, it is recommended to include more days to be modelled in the summer and winter seasons also to include more seasons other than the studied seasons. In addition, it is recommended for further improvement in the study, to compare between the actual measured data from the site with the CALPUFF simulation results. [1]

#### Declaration of conflicting interests

The authors declared no conflicts of interest with respect to concerning the authorship and/or publication of this article.

#### Data availability statement

The data that support the findings of this study are available from the corresponding author, Sabah Abdul-Wahab, upon reasonable request.

#### Funding

The authors received no financial support for the research and/or authorship of this article.

#### References

- [1] Olusegun, O., Adeniyi, A., Adeola, G., *Impact of Granite quarrying on the health of workers and nearby residents in Abeokuta Ogun State, Nigeria*. Ethiopian Journal of Environmental Studies and Management, 2(1), 2009.
- [2] Sayara, T., Hamdan, Y., Basheer-Salimia, R., *Impact of air pollution from quarrying and stone cutting industries on agriculture and plant biodiversity*. Resources and Environment, 6, 122–126, 2016.
- [3] Sayara, T., *Environmental impact assessment of quarries and stone cutting industries in Palestine: case study of Jammain*. Journal of Environment Protection and Sustainable Development, 2(4), 32–38, 2016.
- [4] Latha, K. M., Highwood, E. J., *Studies on particulate matter (PM<sub>10</sub>) and its precursors over urban environment of Reading, UK*. J. Quant. Spectrosc. Radiat. Transf., 101, 367–379, 2006.
- [5] Carugno, M., Dentali, F., Mathieu, G., Fontanella, A., Mariani, J., Bordini, L., Milani, G. P., Consonni, D., Bonzini, M., Bollati, V., Pesatori, A. C., *PM<sub>10</sub> exposure is associated with increased hospitalizations for respiratory syncytial virus bronchiolitis among infants in Lombardy, Italy*. Environ. Res., 166, 452–457, 2018.
- [6] Song, J., Zheng, L., Lu, M., Gui, L., Xu, D., Wu, W., and Liu, Y., *Acute effects of ambient particulate matter pollution on hospital admissions for mental and behavioral disorders: A time-series study in Shijiazhuang, China*. Sci. Total Environ., 636, 205–211, 2018.
- [7] Weinmayr, G., Pedersen, M., Stafoggia, M., Andersen, Z. J., Galassi, C., Munkenast, J., Jaensch, A., Oftedal, B., Krog, N. H., Aamodt, G., Pyko, A., Pershagen, G., Korek, M., Faire, U. D., Pedersen, N. L., Östenson, C. G., Rizzuto, D., Sørensen, M., Tjønnelund, A., Bueno-de-Mesquita, B., Vermeulen, R., Eeftens, M., Concin, H., Lang, A., Wang, M., Tsai, M. Y., Ricceri, F., Sacerdote, C., Ranzi, A., Cesaroni, G., Forastiere, F., Hoogh, K., Beelen, R., Vineis, P., Kooter, I., Sokhi, R., Brunekreef, B., Hoek, G., Raaschou-Nielsen, O., Nagel, G., *Particulate matter air pollution components and incidence of cancers of the stomach and the upper aerodigestive tract in the European study of cohorts of air pollution effects (ESCAPE)*. Environment International 120, 163–171, 2018.
- [8] Abril, G. A., Diez, S. C., Pignata, M. L., and Britch, J. *Particulate matter concentrations originating from industrial and urban sources: Validation of atmospheric dispersion modeling results*. Atmospheric Pollution Research, 7(1), 180–189, 2016.
- [9] Abdul-Wahab, S. A., Charabi, Y., Osman, I. I., Al-Rawas, G. A., Fadlallah, S. O. *Impact of the ambient air quality due to the dispersion of PM<sub>10</sub> from a hot-dip galvanizing plant located in the Sultanate of Oman*. Air Qual. Atmos. Health. 2019a.
- [10] Abdul-Wahab, S., Fadlallah, S., and Al-Rashdi, M., *Evaluation of the impact of ground-level concentrations of SO<sub>2</sub>, NO<sub>x</sub>, CO, and PM<sub>10</sub> emitted from a steel melting plant on Muscat, Oman*. Sustain. Cities Soc., 38, 675–683, 2018.
- [11] Joneidi, N., Rashidi, Y., Atabi, F., Broomandi, P., *Modeling of air pollutants' dispersion by means of CALMET/CALPUFF (case study: District 7 in Tehran city)*. Pollution., 4(2), 349–357, 2018.
- [12] Rojano, R., Arregocés, H., Angulo, L., and Restrepo, G., *PM<sub>10</sub> emissions due to storage in coal piles in a mining industrial area*. Air Pollution XXIV. 2016.
- [13] Pratama, A. *Investigation of air pollution dispersion from kiln stacks based on seasonal using multi-model integration (WRF/CALPUFF)*. IOP Conference Series: Earth and Environmental Science, 2021.
- [14] Xie, L., Xu, Q., He, R., *Atmospheric pollution impact assessment of brick and tile industry: a case study of Xinmi City in Zhengzhou, China*. Sustainability, 13(4), 2414, 2021.
- [15] Abdul-Wahab, S. A., Fadlallah, S. O., Al-Riyami, M., Al-Souti, M., Osman, I. A., *study of the effects of CO, NO<sub>2</sub>, and PM<sub>10</sub> emissions from the Oman Liquefied Natural Gas (LNG) plant on ambient air quality*. Air Qual. Atmos. Health., 13(10), 1235–1245, 2020.
- [16] Otero-Pregueiro, D., Hernández-Pellón, A., Borge, R., Fernández-Olmo, I. *Estimation of PM<sub>10</sub>-bound manganese concentration near a ferromanganese alloy plant by atmospheric dispersion modelling*. Sci. Total Environ., 627, 534–543, 2018.
- [17] Zhou, Y., Levy, J. I., Hammitt, J. K., Evans, J. S., *Estimating population exposure to power plant emissions using CALPUFF: A case study in Beijing, China*. Atmospheric Environment, 37(6), 815–826, 2003.
- [18] Tartakovsky, D., Broday, D. M., and Stern, E. *Evaluation of AERMOD and CALPUFF for predicting ambient concentrations of total suspended particulate matter (TSP) emissions from a quarry in complex terrain*. Environ. Pollut., 179, 138–145, 2013.
- [19] Tartakovsky, D., Stern, E., Broday, D. M. *Dispersion of TSP and PM<sub>10</sub> emissions from quarries in complex terrain*. Sci. Total Environ., 542, 946–954, 2016.
- [20] Kunooz Gabbro. Resources. Retrieved October 15, 2019, from <http://kunoozgabbro.com/quarry/#resources>
- [21] Kunooz Gabbro. Mining and Quarrying. Retrieved October 15, 2019, from <http://kunoozoman.com/mining-and-quarrying/>
- [22] Kunooz Gabbro. Kunooz Gabbro Welcomes You. Retrieved January 1, 2019, from <http://kunoozgabbro.com/>
- [23] Ministry of Commerce and Industry. Development of the manufacturing industries of oman preparing for the future. Analytical Report. 2015.
- [24] NOAA/ESRL Radiosonde Database. Mark Govett. Retrieved October 1, 2019, from <https://ruc.noaa.gov/raobs/>
- [25] Abdul-Wahab, S., Fadlallah, S., Alnaamani, A., *Impact of NO<sub>x</sub> emissions released from a gas turbine-based power plant on the*

- ambient air quality*. Environ. Forensics., 20(1), 50-65, 2019.
- [26] Charabi, Y., Abdul-Wahab, S., Al-Rawas, G., Al-Wardy, M., Fadlallah, S., *Investigating the impact of monsoon season on the dispersion of pollutants emitted from vehicles: A case study of Salalah city, Sultanate of Oman*. Transp. Res. D Transp. Environ. 59, 108-120, 2018.
- [27] Abdul-Wahab, S. A., Fgaier, H., Elkamel, A., Chan, K., *Air quality assessment for the proposed miller Braeside quarry expansion in Canada: TSP*. Air Qual. Atmos. Health., 8(6), 573-589, 2015.
- [28] U.S. Environmental Protection Agency. Air and radiation: national ambient air quality standards (NAAQS). 2012.